Next Energy 11 (2026) 100552

Contents lists available at ScienceDirect

Next Energy

journal homepage: www.sciencedirect.com/journal/next-energy

Research article

Robust optimization of a battery-supercapacitor microgrid under load demand uncertainty

Md. Rashidul Islam[a], Arafat Ibne Ikram[b,*], Md Ahad Uddin[b], Rizvi Ahamed[b]

[a] Department of Electrical and Electronic Engineering, Noakhali Science and Technology University, Noakhali 3814, Bangladesh
[b] Department of Electrical and Electronics Engineering, International Islamic University Chittagong, Chittagong 4318, Bangladesh

ARTICLE INFO

Keywords:
Renewable energy generation
Economic analysis
Life cycle assessment
Optimization
Load demand intermittency

ABSTRACT

Rising energy demand and global threats from fossil fuels necessitate the adoption of renewable energy sources (RES) to harness free resources and reduce carbon emissions. The optimal size and power exchange of grid-connected RES and hybrid energy storage systems are investigated with the primary optimization objective for a city in Bangladesh. The total number of solar photovoltaic panels, wind turbines, supercapacitors, and lithium-ion batteries is considered a decision factor in the proper size of the hybrid renewable system. A probability density function combines the uncertainty with the previously gathered load demand. One of the primary constraints is accounting for load demand intermittency while optimizing the per-unit cost of energy. By utilizing an energy management system, the energy balance between the microgrid and the conventional grid is controlled under a supervised approach. A mathematically designed objective function is used to optimally design the hybrid system, with 3 objectives in mind: net present cost, levelized cost of energy (LCoE), and renewability. The LCoE is found to be $0.11/kWh for the proposed system. The results show that although the per-unit cost of energy is lower in the conventional grid, the proposed microgrid model can fulfill the energy demand solely using renewable generation.

1. Introduction

The globe has been using a lot more power lately, mostly from fossil fuels, due to factors like industrial development, increasing numbers of people, and the need for personal comfort. This energy demand and the associated CO_2 emissions are expected to continue. For example, between 2010 and 2016, global population, power consumption, and carbon dioxide emissions increased significantly (7.4%, 9.1%, and 6.0%, respectively) [1,2]. The building sector, which consumes a significant amount of electricity, is responsible for 36% and 38% of greenhouse gas emissions in Europe and the US, respectively, and for 40% and 39% of electrical consumption globally [3]. Given this, the main concerns about the world's electricity supply are the volatility of fossil fuel prices, their depletion, and the release of carbon dioxide that results from them. To address the growing need for energy, reduce the cost of power in remote areas, and minimize the impact on the environment, this scenario has forced and inspired researchers, companies, and experts to create and incorporate sources of clean energy.

In hybrid systems, size minimization and control of energy are critical challenges. Various studies on these themes have been conducted, including energy storage analysis in size problems [4], device sizing [5], and regulatory capabilities in microgrids [6,7], optimal sizing of lithium battery energy storage in grid-connected mode, and multi-operation management in hybrid systems [8,9]. A size management issue determines the ideal size of each element with the given criteria. Many objectives, such as cost [10], effective-response time [11], performance [12], and reliability, can be stated for the size minimization issue. The size minimization of hybrid systems has been tackled in 2 frameworks in the literature: single-objective [13] and multi-objective [14]. The majority of research has treated dimension minimization as a single-objective issue. The size dilemma can be handled using both classical and meta-heuristic techniques [15–18,19]. In addition to requiring a significant amount of computing time, classical algorithms depend on the original answer and require derivative information. These algorithms may be stuck in local optima. Meta-heuristic algorithms, contrary to conventional approaches, are probabilistic search methods that are derivative-free. These algorithms can avoid probable local optima

* Corresponding author.
E-mail addresses: rashidulislam.eee@nstu.edu.bd (Md. R. Islam), arafatibne.ikram@gmail.com (A.I. Ikram), kahad402@gmail.com (M.A. Uddin), rizviahamed7171@gmail.com (R. Ahamed).

https://doi.org/10.1016/j.nxener.2026.100552
Received 20 March 2025; Received in revised form 15 February 2026; Accepted 18 February 2026

Nomenclature

Φ_{solar}	Rated capacity of a solar module (W)
Φ_{wind}	Rated wind turbine power (kW)
Ψ	Solar irradiance at time t (W/m^2)
$\upsilon_{in,rate,out}$	Cut-in, rated, and cut-off wind speeds (m/s)
τ	Project lifetime
X_{solar}	Number of solar panels
X_{widn}	Number of wind turbine
X_{bat}	Number of battery capacity
X_{sc}	Number of super-capacitor capacity
SoC	State of charge
$MEMS$	Microgrid Energy Management System
GOA	Grasshopper Optimization Algorithm
$LCoE$	Levelized cost of energy ($\$/kWh$)
NPC	Net present cost ($\$$)
CRF	Capital Recovery Factor
RES	Renewable Energy Sources

by striking an appropriate equilibrium between diversity and amplification. Due to their effectiveness, meta-heuristic algorithms have grown increasingly popular compared to traditional approaches for tackling size issues. The ideal size of a grid-connected photovoltaic (PV)-wind hybrid structure has been determined in Ref. [20]. The outcomes suggest that the grid-dependent hybrid network is cost-effective. In Ref. [21], the best configuration for a PV-wind-battery combination was addressed, and the findings suggest that demand response strategies can lower the size of energy storage systems. The size challenge for a grid-connected and off-grid PV-biomass hybrid system was examined in Ref. [22]. The results reveal that a system linked to the grid outperforms the disconnected solution. In Ref. [23], the best size for a grid-connected PV-wind-battery combined system was determined, and the findings show that access to the grid is helpful from a financial point of view. The best size for a grid-connected PV-battery hybrid system was discovered in Ref. [24], and the quantity of PV panels, batteries, and inverters was chosen as a choice factor. In Ref. [25], battery storage sizing for a grid-dependent PV-battery hybrid appliance under several circumstances was determined, and the ideal size was determined for each case. The best size for a PV-wind-battery hybrid system was determined in Ref. [26], and the findings reveal that the cost of the system is significantly impacted by the starting cost of PV and the retail cost for environmentally friendly power. The storage size and operating problems for a PV-battery hybrid system were explored in Ref. [27,28].

Microgrids offer a promising solution for integrating renewable energy sources (RES) and enhancing grid flexibility [29,30]. However, 2 major limitations remain in the current body of research— First, most existing studies either assume deterministic load profiles or apply basic time-series models that fail to reflect the probabilistic nature of real-world energy consumption. For example, a stand-alone study incorporated demand uncertainty but did not address generation cost optimization [31]. Similarly, a hydrogen-based hybrid microgrid model was proposed but ignored demand-side variability [32–34], limiting its adaptability in real-time operations. Second, the majority of prior works rely on single-layer energy storage systems [35–38], predominantly lithium-ion batteries. While effective for bulk storage, batteries alone struggle with frequent charge-discharge cycles and rapid response demands. Supercapacitors, though less energy-dense, excel in high-frequency cycling scenarios. Despite their complementary benefits [39–41], dual-layer hybrid storage systems are rarely explored in conjunction with load uncertainty modeling. Moreover, many models assume stand-alone microgrid topologies and do not simulate real-time energy exchange with conventional grids under high-resolution temporal settings (e.g., 8760 h in a year), which makes their applicability to developing countries, where grid dependency and variability are critical and limited.

To overcome these challenges, the present study proposes an optimal sizing considering the uncertainty of load demand and at least half the penetration of grid energy with RES. In contrast, this approach integrates a dual-layer hybrid energy storage system (HESS) under minimum operation cost using a guided energy management system. The key contributions of this work are:

- A novel hybrid energy storage configuration integrating batteries and supercapacitors is developed to enhance the responsiveness and reliability of dynamic microgrid operations.
- A probabilistic load demand model is implemented to consider uncertainty in energy consumption, enabling more realistic and resilient capacity planning.
- A logic-based Energy Management System for real-time energy balancing, integrated with a robust optimization framework targeting the minimization of per-unit energy cost.
- A comprehensive techno-economic and environmental evaluation, for demonstrating the cost-effectiveness and carbon mitigation potential of the proposed system under practical operating conditions.

These contributions aim to provide innovative, scalable solutions for sustainable energy systems in both developing and developed regions. Furthermore, this study diverges from the prevalent assumption of stand-alone microgrid architectures by explicitly modeling a grid-connected configuration, reflecting practical energy policy and infrastructure realities in developing regions.

This paper is structured as follows: Section 1 introduces the key themes and significance of the study; Section 2 details the construction of models for PV, wind, energy storage, economic assessment systems, and grid energy balance calculations; Section 3 examines the effects of load demand uncertainty; Section 4 explores strategies for effective energy management; Section 5 describes the algorithms used to optimize system performance; Section 7 interprets the outcomes of the study, highlighting key findings; Section 8 summarizes the main points and offers future recommendations.

2. Model development

The configuration of the proposed microgrid, as shown in Fig. 1, consists of solar photovoltaic panels, wind turbines, energy storage units such as lithium-ion battery and super-capacitor, and the electrical load demand model incorporated with the microgrid energy management system (MEMS). The proposed methodological approach comprises mainly 2 parts. Firstly, the technical model is designed for hourly energy calculation and tabulation for each RES, and secondly, the economic model for life cycle cost assessment for each used component, considering interest and inflation rates. Hourly solar irradiance will dictate how much energy will be produced in each solar panel, and inverter efficiency affects how much energy will be converted from Direct Current power to Alternating Current power. The wind coefficient and turbine rating specifications determine how much wind energy can be harnessed from the given wind speed data. After summing the total energy from RES, the MEMS will compare each hour with the energy balance equation and decide if the control system will store the energy in the energy storage bank, use the stored energy from the battery bank, or it will exchange energy with the conventional grid setting. The electrical load model that is considered here is based on the intermittency of load demand. This constraint will overrule real-time energy balancing through different energy sources and reservoirs. A probability density function (PDF) is used to determine the uncertain load under the given constraints and load curve. The Gaussian distribution is applied to transform the load uncertainty for annual load demand calculation. The optimization algorithm will check different solutions to solve the objective function, and after fulfilling the boundary constraints, the final solutions will be considered in the economic model to calculate the overall economic

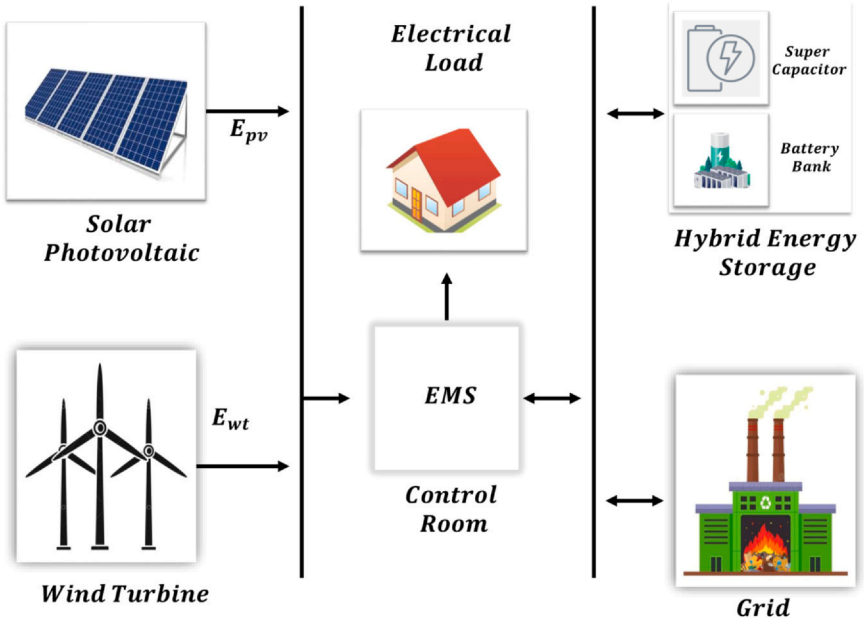

Fig. 1. Configuration of the designed microgrid. EMS = energy management system.

profile. In this particular section, each model is discussed comprehensively with its appropriate mathematical model.

2.1. Solar model

The hourly energy generation (G_{pv}) of solar PV with respect to hourly radiation, $\Psi(t)$, is estimated using Eq. (1) [8,42].

$$G_{pv}(t) = X_{pv} \times \begin{cases} \Phi_{PV} \times \left(\frac{\Psi^2(t)}{R_s - R_c}\right) & \forall \quad 0 \le \Psi(t) < R_c \\ \Phi_{PV} \times \left(\frac{R_a(t)}{R_s}\right) & \forall \quad R_c \le \Psi(t) < R_s \\ \Phi_{PV} \text{ Otherwise} \end{cases} \tag{1}$$

Here, t is the hourly variable, R_C is the cut-off solar radiation, R_S is the maximum possible solar radiation level, and Φ_{PV} is the rated power of the selected solar photovoltaic panels. Solar radiation's threshold data are provided by the PV panel manufacturers. X_{pv} is the optimal size required for the solar photovoltaic panel to run economically, which will be determined by the optimization algorithm. Economic analysis of solar photovoltaic panels is done using the economic model of solar photovoltaic panels. The overall cost of investing, installing, running, and maintaining a solar panel system, discounted to its present value, is referred to as the total solar cost (NPC_{pv}) of solar panels [27,42]. The net present cost (NPC) of PV panels is estimated using Eq. (2).

$$NPC_{solar} = IC_{solar} + O\,\&\,MC_{solar} - Salvage_{solar} \tag{2}$$

The investment cost of PV (IC_{pv}) includes the price of all units, including the installation, the operation and maintenance cost, and any other associated costs, for purchasing and installing the solar panel system as shown in Eq. (3).

$$IC_{solar} = X_{solar} \times \alpha_{solar} \tag{3}$$

The operating and maintaining costs of solar panels ($O\&MC_{solar}$) throughout their expected lifetime are estimated using Eq. (4).

$$O\,\&\,MC_{solar} = X_{solar} \times \beta_{solar} \times \sum_{X_{solar}=1}^{X_{solar}^{max}} \left(\frac{1+\lambda_{solar}}{1+ir}\right)^{\tau} \tag{4}$$

The predicted salvage value of PV panels ($Salvage_{solar}$) is when panels reach the end of their useful life, is calculated as shown in shown Eq. (5).

Table 1
Technical and economical parameter of the PV model [43]

Technical parameter		Economical parameter	
Φ_{pv}	375 (W)	α_{pv}	\$267 (Per Unit)
R_s	1000 (W/m^2)	β_{pv}	$0.01\alpha_{pv}$
R_c	150 (W/m^3)	δ_{pv}	$0.5\alpha_{pv}$
Lifespan (τ)	20 years	λ_{pv}	0.09

$$Salvage_{solar} = X_{solar} \times \delta_{solar} \times \left(\frac{1+\lambda_{solar}}{1+ir}\right)^{\tau} \tag{5}$$

Here, τ is the projected lifespan, ir = 8% is the interest rate, α_{solar} is the per unit capital cost, β_{solar} per unit maintenance cost, δ_{solar} per unit salvage value cost, and λ_{solar} per unit escalation rate that is given in Table 1. X_{solar} is the optimal size required for the solar PV panel to run economically, which will be determined by the optimization algorithm.

2.2. Wind model

The quadratic function of wind velocity (υ) is used to estimate the energy generation (G_{wind}) by the wind turbine model using Eq. (6) [43].

$$G_{wind}(t) = X_{wind} \times \begin{cases} \Phi_{wind}\left(\frac{\upsilon - \upsilon_{in}}{\upsilon_{rate} - \upsilon_{in}}\right) & \forall \quad \upsilon_{in} \le \upsilon \le \upsilon_{rate} \\ \Phi_{wind} & \forall \quad \upsilon_{rate} < \upsilon < \upsilon_{out} \\ 0 & \forall \quad \upsilon < \upsilon_{in} \text{ and } \upsilon > \upsilon_{out} \end{cases} \tag{6}$$

Here, υ_{rate}, υ_{in}, and υ_{out} are the rated speed, cut-in wind speed, and cut-off wind speed of Φ_{wind} power-rated wind turbine provided in Table 2, which are provided by wind turbine manufacturers. The NPC of the

Table 2
Technical and economical parameter of wind turbine [8,43]

Technical parameter		Economical parameter	
Φ_{wind}	3.5 (kw)	α_{wind}	\$267 (Per Unit)
υ_{rate}	11 (m/s)	β_{wind}	$0.02\alpha_{wind}$
υ_{in}	2.8 (m/s)	γ_{wind}	$0.1\alpha_{wind}$
υ_{out}	22 (m/s)	λ_{wind}	0.085
Lifespan (τ)	20 years	ir	8%

wind turbine (NPC_{wind}) is determined by weighing all expenses and benefits related to its installation, use, and maintenance throughout its predicted lifetime. The NPC of the wind model is valued using Eq. (7).

$$NPC_{wind} = IC_{wind} + O\,\&\,MC_{wind} + RC_{wind} - Salvage_{wind} \tag{7}$$

The up-front expenses associated with installing the wind turbine system should be calculated as the investment cost (IC_{wind}) of the wind model is valued using Eq. (8).

$$IC_{wind} = X_{wind} \times \alpha_{wind} \tag{8}$$

The expenditures for maintenance, repairs, monitoring, coverage, and other routine operational expenses are included in the estimation of the wind turbine's operating and maintenance costs ($O\&MC_{wind}$) as shown in Eq. (9).

$$O\,\&\,MC_{wind} = X_{wind} \times \beta_{wind} \times \sum_{X_{wind}=1}^{X_{wind}^{max}} \left(\frac{1+\lambda_{wind}}{1+i}\right)^{\tau} \tag{9}$$

The cost of replacing a faulty wind turbine with a new one that has comparable capacity and capabilities is referred to as the replacement cost of a wind turbine (RC_{wind}). Replacement costs for the depreciated wind turbines are estimated using Eq. (10).

$$RC_{wind} = X_{wind} \times \gamma_{wind} \times \sum_{n=5,10,15}^{X_{wind}^{max}} \left(\frac{1+\lambda_{wind}}{1+ir}\right)^{\tau} \tag{10}$$

The salvage value of wind turbines ($Salvage_{wind}$) is the estimated value of an asset after depreciation is complete in its lifespan and is calculated using Eq. (11).

$$Salvage_{wind} = X_{wind} \times \delta_{wind} \times \left(\frac{1+\lambda_{wind}}{1+ir}\right)^{\tau} \tag{11}$$

Here, τ is the projected lifespan of the wind turbine, α_{wind} is the per unit capital cost, β_{wind} is the per unit maintenance cost, γ_{wind} is the replacement cost, and λ_{wind} is the escalation rate as shown in Table 2. X_{wind} is the optimal size required for the wind turbine to run economically feasible for that selected site, which will be determined by the optimization algorithm.

2.3. Hybrid energy storage

The economic assessment model analyses the battery bank's financial performance, whereas the mathematical model of lithium-ion battery packs describes the energy stored and extracted from the battery. The spontaneous state of charge (B_{SoC}) of the total battery pack is calculated using Eq. (16). Battery charging rate (B_C), and the discharging rate (B_D) is estimated using Eq. (15).

$$SoC_{SC}(t) = \frac{V_s c}{V_m ax} \tag{12}$$

$$SoC_{bat}(t) = \frac{V_s c}{V_m ax} \tag{13}$$

$$U_{total} = E_{oc} - U_{act} - U_{ohmic} \tag{14}$$

with

$$\begin{cases} E_{oc} = K_c\left[E_c + (T-298)\frac{-44.43}{zF} + \frac{RT}{zF}\ln\left(P_{H_2}P_{O_2}^{1/2}\right)\right] \\ U_{act} = \frac{1}{\tau s+1}.\, NA_{nom} ln\left(\frac{i_{fc}}{i_0}\right) \\ U_{ohmic} = R_{internal}.\, i_{fc} \end{cases} \tag{15}$$

$$B_{SOC}(t) = B_{SOC}(t-1) + \frac{\eta_C(t).\, B_C.\, \Delta t}{C_{battery}} + \frac{B_D(t).\, \Delta t}{\eta_D.\, C_{battery}} \tag{16}$$

Here, ΔT is the time difference, $B_{SOC}(t)$ is the spontaneous SOC, $C_{battery} = 100aH$ is the capacity, $\eta_C = 90\%$ is the battery charging efficiency, $\eta_D = 95\%$ is the battery discharging efficiency, as shown in Table 3.

Table 3
Technical and economical parameter of battery and super-capacitor [43]

Technical parameter		Economical parameter	
Capacity (Battery)	1.2kWh (12 V, 100Ah)	$\alpha_{battery}$	\$35 (Per Unit)
Capacity (capacitor)	0.6kWh (6 V, 100Ah)	$\alpha_{capacitor}$	\$60 (Per Unit)
$\eta_C^{battery}$	95%	$\gamma_{battery}$	$0.01*\alpha_{battery}$
$\eta_C^{capacitor}$	99%	$\gamma_{capacitor}$	$0.02*\alpha_{capacitor}$
$\eta_D^{battery}$	92%	$\lambda_{battery}$	0.085
$\eta_D^{capacitor}$	99%	$\lambda_{capacitor}$	0.138
Lifespan (τ)	10 years	ir	8%

$$SOC_{min} \le SOC(t) \le SOC_{max}$$

Spontaneous SOC of the battery is kept between $SOC_{min} = 20\%$ of $C_{battery}$ and $SOC_{max} = 80\%$ of $C_{battery}$ for battery life longevity [16,44].

The NPC of the battery bank ($NPC_{battery}$) is determined by considering all of the expenses and benefits related to its installation, use, and maintenance throughout the project lifespan is calculated using Eq. (17).

$$NPC_{battery} = IC_{battery} + RC_{battery} - Salvage_{battery} \tag{17}$$

The up-front expenses associated with acquiring and installing the battery bank system ($IC_{battery}$) are calculated using Eq. (18).

$$IC_{battery} = X_{battery} \times \alpha_{battery} \tag{18}$$

The cost of replacing a faulty battery with a new one that has comparable capacity and capabilities is the replacement cost of a battery ($RC_{battery}$) that is estimated using Eq. (19).

$$RC_{battery} = X_{battery} \times \gamma_{battery} \times \sum_{n=5,10,15}^{X_{wind}^{max}} \left(\frac{1+\lambda_{battery}}{1+ir}\right)^{\tau} \tag{19}$$

The salvage value of the battery bank ($Salvage_{battery}$) is the estimated value of an asset after depreciation is complete in its lifespan and it is calculated using Eq. (20).

$$Salvage_{battery} = X_{battery} \times \delta_{battery} \times \left(\frac{1+\lambda_{battery}}{1+ir}\right)^{\tau} \tag{20}$$

Here, τ is the projected lifespan of the batteries, $\alpha_{battery}$ is the per unit capital cost, $\gamma_{battery}$ is the replacement cost, $\lambda_{battery}$ is the escalation rate of the battery bank that is given in Table 3. The optimization method will determine $X_{battery}$, the ideal size needed for the battery bank to operate profitably.

2.4. Economic assessment

Economic assessment considers the cost of electrical energy produced and determines the price it should be sold to break even during its operational period.

2.5. Total net present cost (TNPC)

The TNPC is composed of the NPC of all the components used in microgrids, such as PV panels, wind turbines, batteries, and supercapacitors, with a summation of their respective capital cost and maintenance cost minus the salvage value, which is estimated using Eq. (21).

$$TNPC = NPC_{solar} + NPC_{wind} + NPC_{battery} + NPC_{sc} \tag{21}$$

2.6. Capital recovery factor (CRF)

The CRF is the ratio of a fixed annuity to its estimated value over a specific length of time, which is evaluated using Eq. (22) [43].

Table 4
BPDB per unit electricity prices [45]

Operation	Price ($ /kWh)
Conventional energy retail ($Grid_{buy}$)	0.05
Renewable energy selling ($Grid_{sell}$)	0.05

BPDB = Bangladesh Power Development Board.

$$CRF = \frac{ir \times (1 + ir)^{\tau}}{(1 + ir)^{\tau} - 1} \tag{22}$$

2.7. Levelized cost of energy (LCoE)

The LCOE is a conventional method for evaluating and comparing electricity generation costs, which indicates the viability of the energy plant. The per unit electricity cost ($\$/kWh$) is calculated using Eq. (23) [20,43]. Here, the annual hourly electrical load consumption is $\sum_{t=1}^{8760} L(t)(kWh)$ (365days × 24 h)

$$LCoE = \frac{CRF \times TNPC - (Grid_{revenue} - Grid_{expense})}{\sum_{t=1}^{8760} Load\,(t)} \tag{23}$$

2.8. Conventional grid energy calculation

The total amount of electrical energy bought and sold to the conventional power grid manually is estimated using Eq. (24). Per-unit exchange rate of the power grid is given in Table 4

$$\begin{aligned} Grid_{revenue} &= \sum_{t=1}^{t=8760} (Grid_{sell} \times selling\ Price) \\ Grid_{expense} &= \sum_{t=1}^{t=8760} (Grid_{buy} \times retail\ Price) \end{aligned} \tag{24}$$

3. Load demand uncertainty analysis

The Gaussian method employs several distribution models, including normal, beta, triangular, and lognormal distributions. In this section, the Load uncertainty model was achieved through normal distributions to analyze levelized costs and uncertain demand. For all buildings, the model necessitates 8760 iterations. Because of its symmetric features about the mean, the normal or Gaussian distribution is the most commonly employed in Monte Carlo simulations [46,47]. The normal distribution's PDF is as shown in Eq. (25)

$$f(x;\, \mu,\, \sigma^2) = \frac{1}{\sqrt{2\pi\sigma^2}} \exp - (x - \mu)^2/2\sigma^2 \tag{25}$$

A standard normal distribution has a mean of zero and a standard deviation of one; the equation for this is as shown in Eq. (26)

$$f(x;\, 0,\, 1) = \frac{1}{\sqrt{2\pi}} \exp - (x/2\sigma^2) \tag{26}$$

The normal distribution's cumulative density function is as shown in Eq. (27).

$$F(x) = \int_{-\infty}^{\infty} \frac{1}{\sqrt{2\pi}} \exp - (x/2\sigma^2) \tag{27}$$

The electrical load data for 24 h, shown in Fig. 2, which was also used in this study, are collected for the Halishahar distribution feeder, which predominantly serves urban residential and institutional buildings, including small businesses, offices, and educational campuses. The load profile reflects typical consumer behavior, with morning and evening peaks due to residential activity and midday consumption from institutional and commercial users. The Gaussian distribution shown in Eq. (27) is multiplied by each hourly load demand to simulate uncertainty in this composite load profile over 8760 iterations (hours in 365 days).

The monthly total load demand of the newly created load model is shown as Fig. 3.

After applying the PDF, the highest load demand is depicted in August, and the lowest is observed in February. In January, the load demand for the Halishahar distribution feeder was around 15,000 MW. After experiencing a sharp fall in February, the total load demand

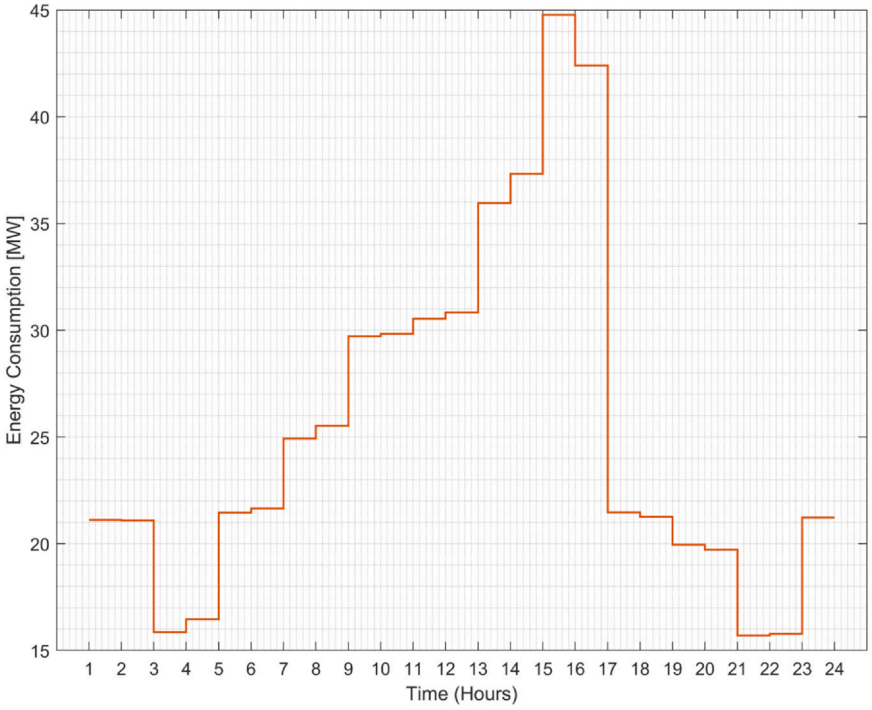

Fig. 2. Average load curve.

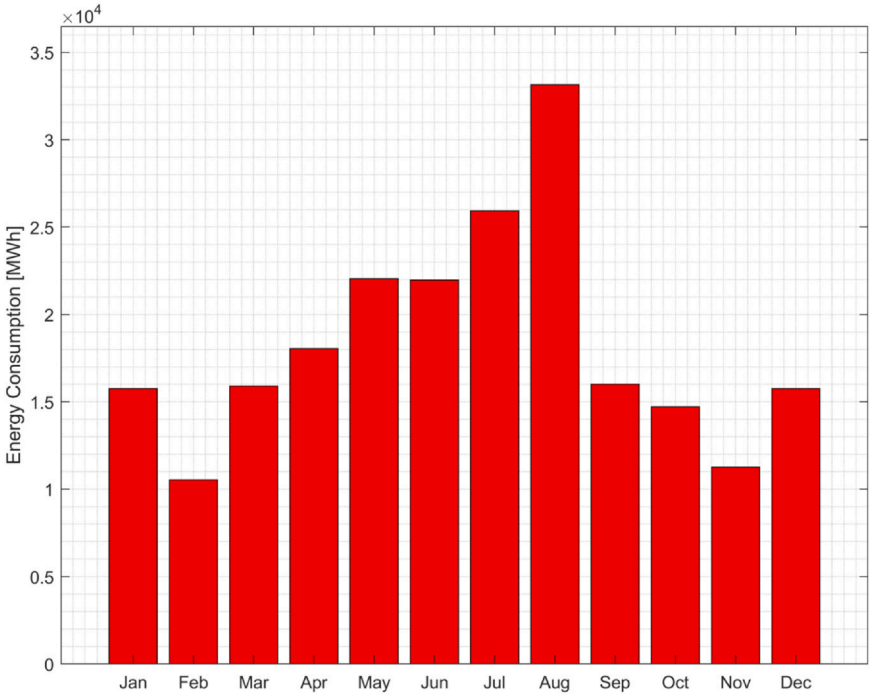

Fig. 3. Monthly load demand.

witnessed a gradual rise till June. After June, the load demand maintained almost a similar level till July. In August, the total load demand peaked and exceeded 30,000 MW. In September, it is seen that the load demand had a dramatic fall and dropped to around 15,000 MW. Till November, load demand experienced a linear decrease, and in December, the load demand increased, exceeding the 15,000 threshold.

4. Microgrid energy management system (MEMS)

MEMS is a sophisticated method of managing energy inside a microgrid, which starts with gathering preliminary data on energy supply and demand. The algorithmic flowchart for the MEMS is shown in Fig. 4. This information is then evaluated to determine if there is a current energy balance surplus or deficit. It assesses energy supply and demand using data before making judgments on surplus storage, redistribution, or alternative sources of energy. The system has decision points and feedback chains to ensure responsiveness to changing conditions, optimize utilization, assure dependability, and possibly successfully incorporate RES.

The surplus energy is first stored in the battery pack. If the battery reaches its limit, then the excess energy is stored in the capacitor, and after that energy is sold at fifty percent of the retail price. Similarly, when generation is lower than consumption, then the energy balance equation checks whether the deficit energy can be taken from the HES. By applying the battery equation, it is calculated how much charge is taken from the HES. Once it checks, the algorithm updates the SOC level of both the battery and super-capacitor. If the HES runs out of energy, then the deficit amount is purchased from the grid. This approach provides effective energy management by maximizing resource utilization while preserving dependability and perhaps incorporating RES. The specifics of each decision point and action phase are determined by the microgrid's requirements and capabilities.

To maintain system stability and ensure reliable energy delivery, the microgrid operates under an hourly energy balance constraint, which is shown in Eq. (28). This equation ensures that the sum of power generation and imports is equal to the total demand, storage charging, and any exported power. The MEMS algorithm makes real-time decisions to satisfy this balance while minimizing operational cost.

$$P_{solar}(t) + P_{wind}(t) + P_{Bat}^{dch}(t) + P_{sc}^{dch}(t) + P_{grid}^{buy}(t) = P_{load}(t) + P_{Bat}^{ch}(t) + P_{sc}^{dch}(t) + P_{grid}^{sell}(t) \quad (28)$$

Here, t is denoted as an hourly vector, P_{solar} is the power generated from the solar panel, P_{wind} is the power generated from the wind turbine, P_{Bat}^{dch} is the power discharged from battery, P_{sc}^{dch} is the power discharged from super-capacitor, P_{grid}^{buy} is the power bought from the conventional grid, P_{load} is the power demand, P_{Bat}^{dch} is the power charged to the battery, P_{sc}^{dch} is the power charged from super-capacitor, P_{grid}^{sell} is the Excess power sold to the power grid.

5. Grasshopper optimization algorithm (GOA)

Optimization is the procedure of determining the most effective values for the variables of a specific issue to minimize or maximize a given objective function. Numerous fields of study have optimization challenges [48,49]. Several measures must be taken to address a challenge related to optimization [50,50]. Few studies show how some optimization approaches perform better in system sizing and economic analysis [51–53].

The swarm seeks food by breaking it down into 2 stages: exploration and exploitation. These stages are depicted in Fig. 5. The swarm searches for sources of food during the searching period. Thus, at this point, the grasshopper's score and fitness values need to be adjusted and computed. During the iteration phase, the most effective option among the options is marked as the best solution.

5.1. Initialization

First, the init function will generate a random population of grasshoppers $X_i(i = 1,2,\ldots,n)$ as set, where n = 100. The boundary variables Max_{iter}, c_{max}, c_{min}, LB, UB, and d for an unattached optimization problem are considered the same as shown in Ref. [54].

5.2. Objective function

The fitness function used to compute the value of fitness for every single grasshopper is as follows in Eq. Eq. (29). The fitness of each

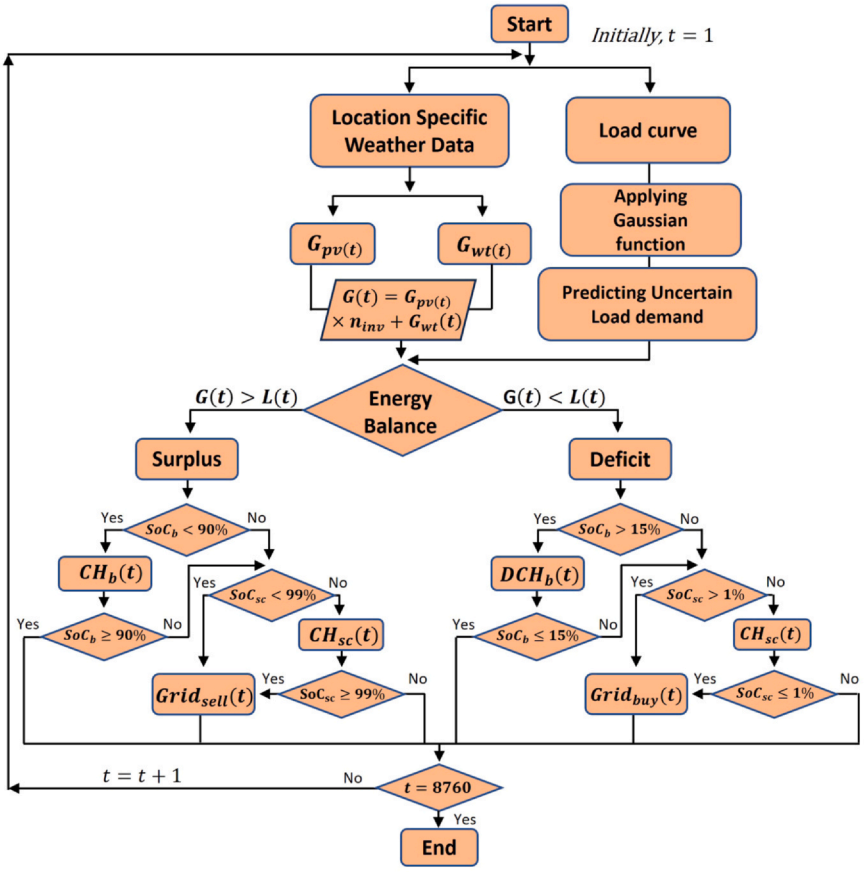

Fig. 4. Algorithmic flowchart for MEMS. MEMS = microgrid energy management system.

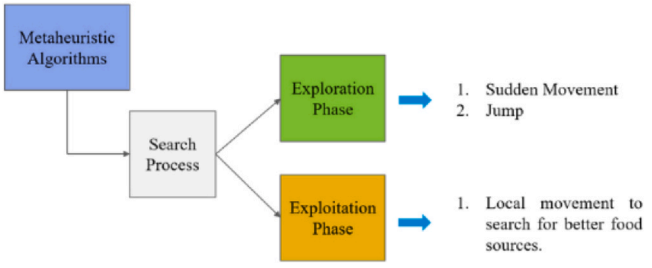

Fig. 5. Swarm stages approach [54].

grasshopper is evaluated using the LCoE as the objective function, as defined in Eq. (29). During each iteration, the algorithm updates the positions of the grasshoppers in the solution space by considering social, gravitational, and wind forces to minimize the LCoE value.

$$f(o) = \frac{CRF \times TNPC - (Grid_{revenue} - Grid_{expense})}{\sum_{t=1}^{8760} Load(t)} \tag{29}$$

In the GOA-based optimization framework, each grasshopper represents a unique candidate solution characterized by a vector of 4 control variables: the installed capacities of Solar PV panels (X_{pv}), Wind Turbines (X_{wind}), lithium-ion batteries ($X_{battery}$), and supercapacitors (X_{sc}). These variables are continuous and bounded within predefined technical and economic ranges shown in EQ. (21).

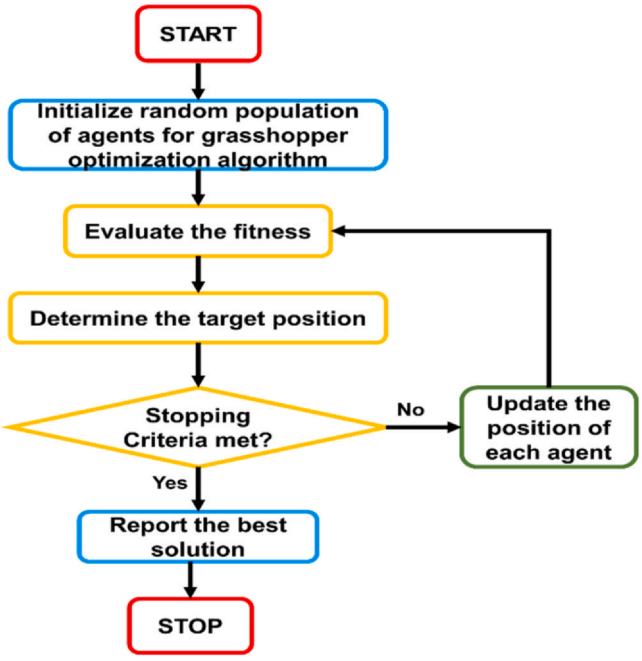

Fig. 6. GOA flowchart [54]. GOA = grasshopper optimization algorithm.

5.3. GOA operation

The algorithmic flowchart shown in Fig. 6 is executed in the following operation, where Table 5 is used as the parameter for the optimization decision and boundary variable.

5.3.1. Optimal solution and condition

The optimal solution for the first iteration with the smallest fitness value across all grasshoppers. The condition is true, as the current iteration has a maximum of 200 iterations.

Table 5
Grasshopper optimization parameter

Parameter	Swarm size	Maximum iteration	Termination criteria	Total program run
Value	10	200	50	3

5.3.2. Normalization of the distance

To normalize the distance between grasshoppers, c is calculated using the following Eq. (30) and (31):

$$\sum_{j=1,i\neq j}^{N} c\frac{UB_d - LB_d}{2} s(|x_j^d - x_i^d|)\frac{|x_j - x_i|}{d_{ij}} \tag{30}$$

$$c = c_{max} - iter\frac{c_{max} - c_{min}}{Max_{iter}} = 1 - 2 \times \frac{1 - 0.00004}{9} \approx 0.80001 \tag{31}$$

The GOA method is a swarm-based strategy that mimics grasshopper social behavior and hunting strategies in nature. Calculating the position of each solution involves calculating 3 forces: social interaction (S_i), wind advection (A_i), and gravity force (G_i), using a mathematical model shown in Eq. (32).

$$X_i = S_i + G_i + A_i \tag{32}$$

where S_i provides the solution's social interaction with the other grasshoppers, G_i indicates the gravitational force on the solution, and A_i represents wind advection. The location of every solution once random behavior has been added and shown in Eq. (33).

$$X_i = r_1 S_i + r_2 G_i + r_3 A_i \tag{33}$$

Here r_1, r_2, and r_3 are random integers in the range [0, 1]. let's have a glimpse at the force models employed, shown in Eq. (33).

5.3.3. Social interaction

Let us begin with the power of social interaction S_i. The following formula reflects the result's social interaction with the different hoppers:

$$S_i = \sum_{j=1}^{N} s(d_{ij})\hat{d_{ij}}, \text{ where } i \neq j$$

$$s = fe^{\frac{-r}{l}} - e^{-r}$$

where $d_{ij} = |x_j - x_i|$ represents the distance between i-th grasshopper and the j-th grasshopper, $\hat{d_{ij}} = \frac{|x_j - x_i|}{d_{ij}}$ represents the unit vector.

5.3.4. Gravity force

The gravitational constant, denoted by -g, and the unit vector $\hat{e_g}$, represent the direction of the Earth's center, that is, using the calculated Gravity Force of the GOA.

$$G_i = -g\hat{e_g}$$

5.3.5. Wind force

Following that, let's look at the power of wind direction, which has a big influence on grasshopper nymphs and adults. Consequently, nymph and adult grasshopper motions are associated with the wind direction bold symbol A_i, as shown in EQ. (5.3.5).

$$A_i = u\hat{e_w}$$

where, the drift constant u denotes and the unit vector of the wind force is $\hat{e_w}$.

5.3.6. Grasshopper position

Grasshopper Position is shown in Eq. (5.3.6). Modifications are proposed to prevent grasshoppers from reaching their comfort zone and swarms from converging to the global optimum, focusing on optimal solutions in the D-th dimension.

$$X_i = \sum_{j=1}^{N} s(d_{ij})\hat{d_{ij}} - g\hat{e_g} + u\hat{e_w} = \sum_{j=1}^{N} s(|x_j - x_i|)\frac{|x_j - x_i|}{d_{ij}} - g\hat{e_g} + u\hat{e_w},$$

where $i \neq j$

where G = 0, A is the optimal solution in the d^th dimension, and the upper and lower limits in the d^th dimension are UB_d and LB_d, respectively. The declining coefficient, represented by variable c, is in charge of lowering the comfort zone, repulsion zone, and attraction zone. The value of c decreases as the number of repetitions increases to balance the stages of discovery and extraction utilizing the grasshopper technique. The formula for c is as follows:

$$c = c_{max} - iter\frac{c_{max} - c_{min}}{Max_{iter}}$$

here c_{max} and c_{min} are the highest and lowest possible values of c, iter is the most recent repetition, and Max_{iter} is the total number of iterations. The grasshopper algorithm initializes parameters and population, evaluates each solution using the fitness function, assigns the best solution, and updates coefficient parameters to shrink attraction, repulsion, and comfort zones. The algorithm divides the search space into repulsion, comfort, and attraction zones, maps distances, updates solutions based on distance, and repeats operations until reaching maximum iterations. Time complexity is related to iterations and agents, with a time complexity of O(n) times Max_{iter}. The algorithm's time complexity is $O(n)$ times Max_{iter}. In every iteration, Improved solutions are filtered out as the finest option, otherwise kept as it is in the previous iteration.

6. Analysis conditions

The Halishahar region of Chattogram, Bangladesh, is selected as the location of the case study. Location-specific meteorological data: solar irradiance, wind speed, and ambient temperature are obtained from the NASA Prediction of Worldwide Energy Resources (POWER) database [55]. These datasets comprise annual hourly values and are used to represent the renewable energy potential of the selected area, as shown in Fig. 7.

7. Results and discussion

7.1. Optimization results

The convergence curve shown in Fig. 8 represents the performance of an optimization algorithm during a microgrid cost reduction operation.

The horizontal axis, iterations, is the repetition of the calculation process to generate an outcome performed by the algorithm. Each iteration is an effort by the algorithm to identify a microgrid configuration that is more cost-effective than the previous one. On the vertical axis is the 'Best-objective value', which indicates the algorithm's preferred conclusion at each point, favorable in this instance, indicating the cheapest cost of microgrid execution. The graph shows the algorithm's performance improvement over each generation, with a downward trend indicating a successful optimization process. The graph includes the specific run, total iterations, evaluations of the objective function, and the optimal value found, 2.0×10^8, which is the lowest possible NPC for the projected microgrid. Steep sections indicate substantial improvements, while flattened end sections suggest the

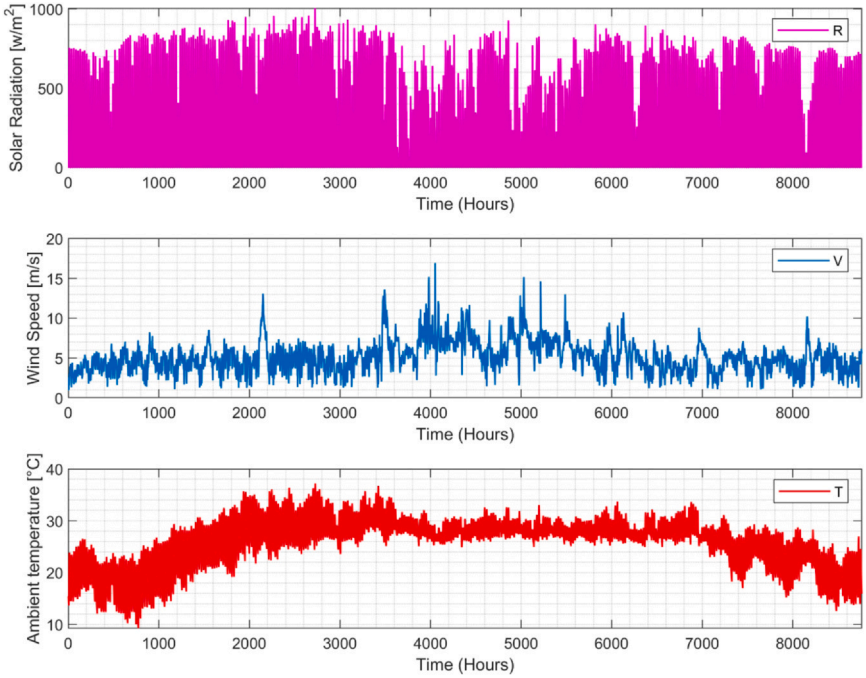

Fig. 7. Meteorological data.

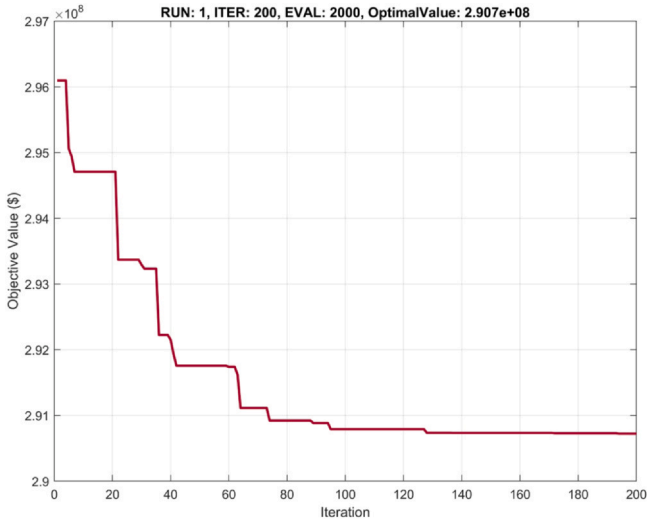

Fig. 8. Convergence Curve.

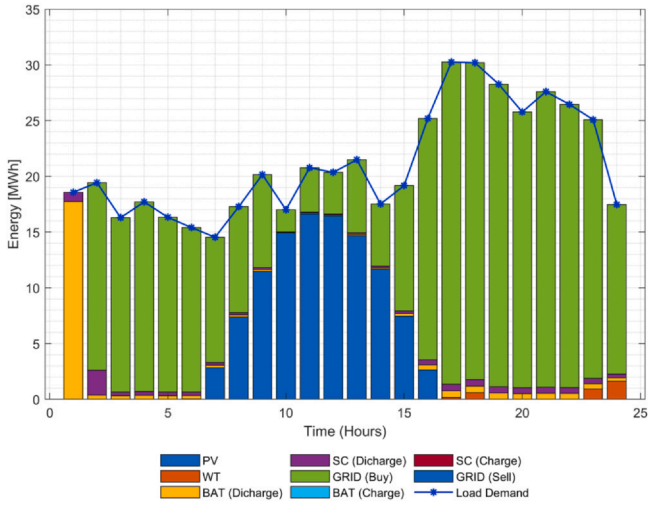

Fig. 9. Generation profile (first day).

algorithm is nearing the optimal solution, making only marginal gains as it refines the result. This is a common pattern in optimization algorithms where initial gains are large and decrease over time.

7.1.1. Computational burden

The optimization framework incorporates high-resolution data (8760 hourly time steps) across solar and wind generation, storage behavior, and grid interactions, creating a high-dimensional search space. Despite this, the total computational time using a swarm size of 10 and 200 iterations of the GOA is recorded as approximately 7 s. The simulation is performed using MATLAB R2023b on a desktop computer equipped with an AMD Ryzen 5 5600 6-core (4.2 GHz) processor and 16 GB RAM. This result demonstrates the computational tractability and efficiency of the proposed model, indicating its viability for near-real-time microgrid configuration tasks.

7.2. Energy profile

The microgrid energy management profile of renewable generation with energy storage and load consumption for the first day is depicted in Fig. 9, which shows the energy distribution for the proposed model for the first 24 h. The majority of the energy generation is supplied from the grid when renewable generation is unavailable, and it is corroborated by the input factors, indicating that there is lower solar radiation during the middle of the year, during the rainy season, which translates to reduced production of solar energy. However, wind speed information reveals a comparable trend.

7.2.1. Renewable generation

The daily generation of solar energy from solar photovoltaic panels is depicted in Fig. 10. The daily total on peak solar generation is witnessed at around 100 MW, and the lowest is seen at around 15 MW.

The daily wind energy generation from wind farms using turbines has been depicted in Fig. 11. However, daily generation is lower in

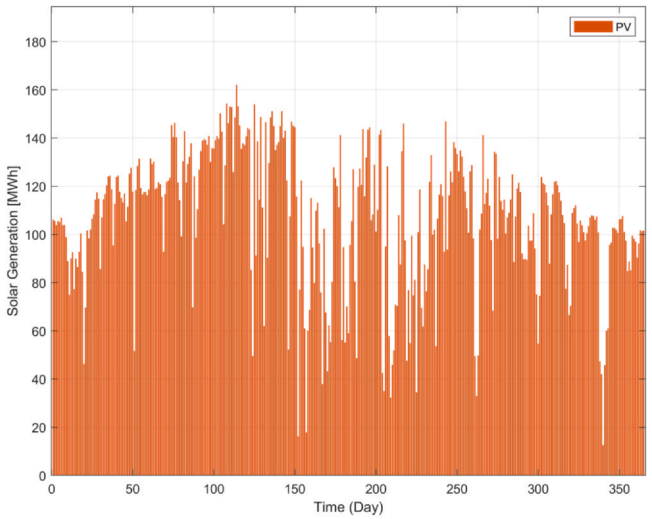

Fig. 10. Daily total solar generation.

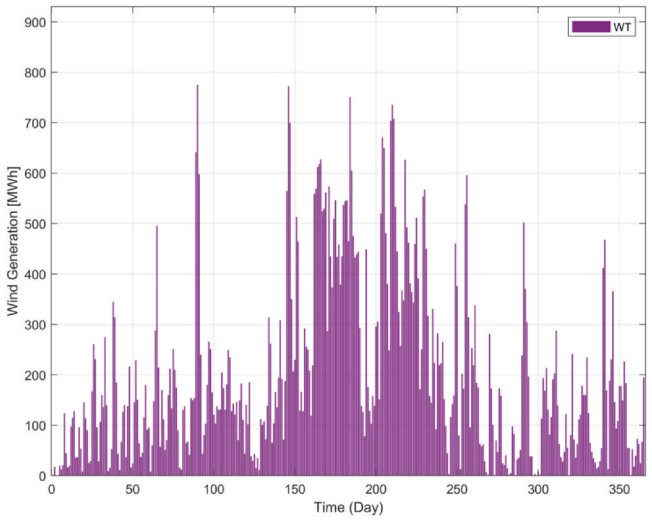

Fig. 11. Daily total wind generation.

wind farms compared to solar plants. Due to lower wind access in the densely populated area like the Halishahar region, total annual wind generation is lower compared to solar.

It is important to note that the peak values shown in Fig. 10 and Fig. 11 represent daily total generation under ideal resource conditions and do not reflect continuous output. These peaks arise due to the mathematical modeling of the generation potential based on standard literature-derived equations and site-specific input data. The average annual energy generation, as shown in Table 6, remains within the plausible range for the region when considering resource variability and system efficiency constraints.

Annual generation and net stored energy in the hybrid energy storage are depicted in Fig. 12. In January, the net generation on the PV is more than 50 MW, while only 20 MW is supplied from the wind turbines because Wind generation is lower than PV generation due to the lower wind access in the selected location. A significant amount of energy is taken from the conventional grid, which is almost 520 MW. The rest of the deficit energy is taken from the lithium battery-super-capacitor hybrid energy storage. PV generation increased till March, after a slight fall, and the PV generation maintained the same level in the following months of April and May. The PV generation saw a slight rise in June and July. On the contrary, the wind generation is higher in June and July compared to PV generation. Peak PV generation is recorded in June, which is around 100 MW, and peak wind generation is recorded in November, where it is around 250 MW total. The energy supplied by the battery and super-capacitor is maintained at the same level throughout the year, due to the intermittent nature of renewable generation.

The generation from solar and wind is irregular throughout the year. To meet the required load demand, the MEMS purchases the shortage of energy from the grid to make the microgrid economically feasible for the designated location. The annual energy generated and provided by different components of the microgrid is plotted in Fig. 13. Fifty percent of the annual energy is provided by the renewable plant, as the selected location has very high solar generation potential, which is around 50%, the second most energy is provided from the conventional grid, which provides around 47%, the energy provided by the lithium energy shortage and super-capacitor is around 2% and 1%, respectively.

7.3. Economic profile

Economic projections take into account the cost of the electrical energy produced and determine the cost at which it should be sold for the system to break even during its operational period. TNPC is broken down into various sectors, they are total capital cost, total maintenance cost, total fuel consumption cost, and the subtraction of salvage value, and it is shown in Fig. 14.

Most of the investment cost goes toward wind turbines, followed by solar panels and energy storage. A moderate amount of money is spent on maintaining the system, which is around $145 Million. The estimated value of an asset after depreciation is shown as the salvage value of the projected system, which is around $145 Million. The total cost of solar panels, wind turbines, super-capacitors, battery banks, and inverters is plotted in Fig. 15, which component holds the majority cost, and which part is less.

7.4. Optimal sizing

The GOA predicts the optimal size of renewable capacity needed to be installed in the microgrid to run the economically feasible configuration shown in Table 6.

The overall economic profile is shown in Table 7. It is seen that $97.34 million needs to be invested as capital cost, $109.8 million will be used as operation and maintenance costs spent over a project lifetime of 25 years. Furthermore, $82.57 million will be used as replacement cost after any component expires its usability after its predicted lifespan. The NPC for the project is found to be around $290.78 million. The LCoE is found to be $0.11/kWh for the proposed system.

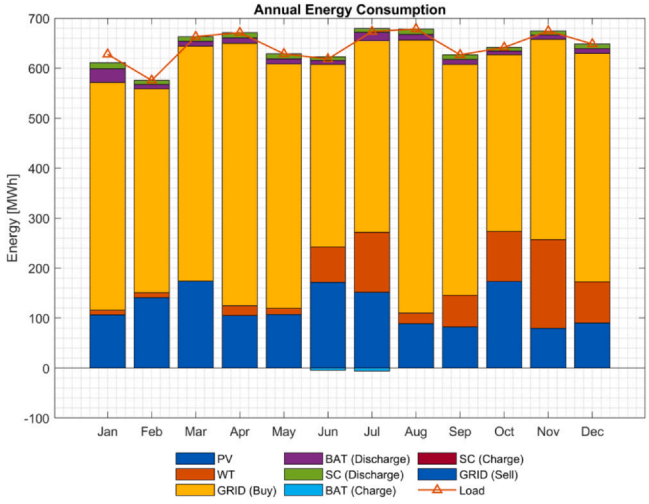

Fig. 12. Annual MEMS profile. MEMS = microgrid energy management system.

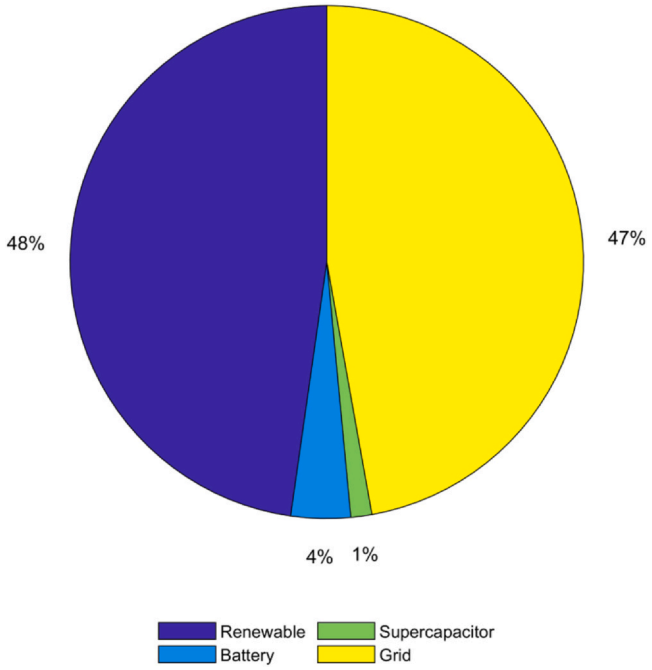

Fig. 13. Gross annual supply.

Table 7 displays the comprehensive economic breakdown. An initial investment of $97.34 million is required for capital costs. Over the 25-year lifespan of the project, operational and maintenance expenses are estimated at $109.8 million. Additionally, $82.57 million is allocated for the replacement of components after they reach the end of their useful life. The TNPC of the project is approximately $290.78 million, and the LCoE is $0.11/kWh.

7.5. Environmental impact

In addition to the techno-economic assessment, the environmental impact of the proposed hybrid microgrid is analyzed in terms of carbon dioxide (CO_2) emission reduction. The baseline emission factor for conventional grid energy in Bangladesh is estimated at 0.80 kg CO_2 per kWh, based on the mix of coal, diesel, and natural gas-based generation [56]. The reduction in CO_2 emissions resulting from a 50% renewable energy penetration into the existing 221.07 GWh conventional energy consumption is around 88.41 kilotons CO_2/year. This environmental benefit complements the economic viability of the system by contributing significantly to the decarbonization of the power sector.

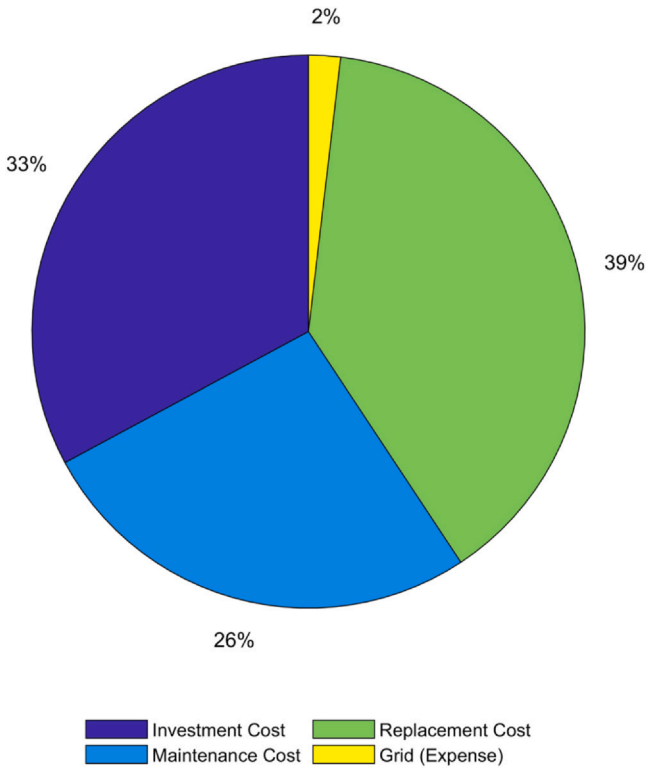

Fig. 15. Distribution of TNPC of the system. TNPC = total net present cost.

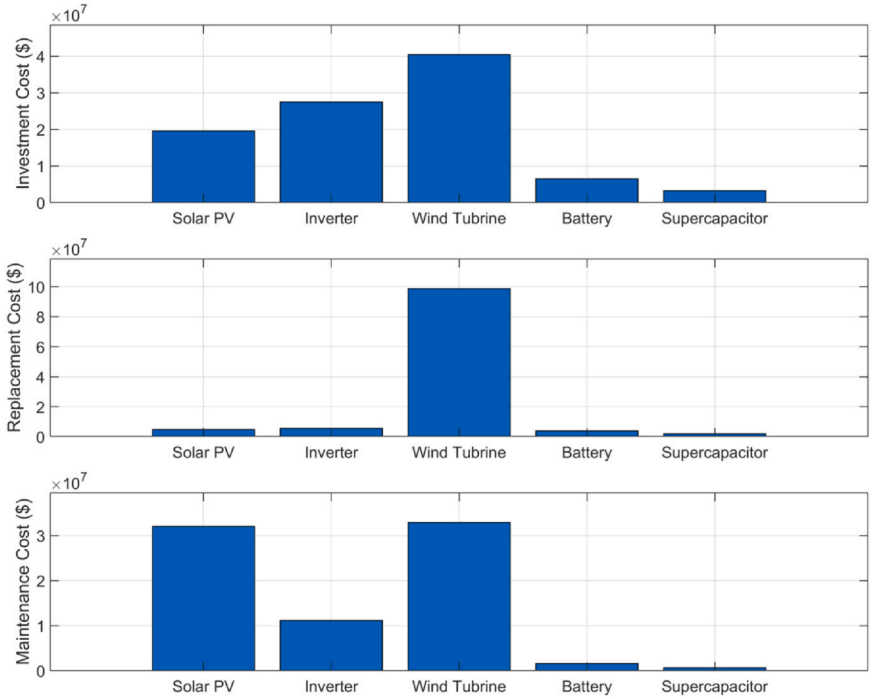

Fig. 14. TNPC of the projected model. TNPC = total net present cost.

Table 6
Microgrid installed capacity and energy profile

Proposed microgrid			Conventional grid	
Name	Required capacity (MW)	Supplied energy (GWh/yr)	Energy status (GWh)	
Solar	19.79	34.66	Load demand	221.07
Wind	34.83	78.38	Grid penetration	50%
Battery	3.48	8.12	Energy provided	6.80
Supercapacitor	0.365	2.45	Energy taken	110.51

Table 7
Microgrid's economic profile

Proposed microgrid					Conventional gird	
Components	Investment cost (million USD)	O&M cost (million USD)	Replacement cost (million USD)	LCoE ($/kWh)	Tariff rate CoE ($/kWh)	
Solar	19.57	32.03	4.80	0.11	Retail	0.05
Wind	40.47	32.93	98.8		Sold	same as retail price
Battery	6.51	1.6	3.92		**Annual report (million USD)**	
Supercapacitor	3.27	0.65	1.97		Expense	5.52
Power inverter	27.52	11.13	5.56		Revenue	0.28
Net present cost		290.78				

LCoE = levelized cost of energy.

Table 8
Comparative studies

Ref.	Study region	Microgrid Structure	Year	LCOE ($/kWh)
[57]	Pakistan	PV, WT, and hydrogen storage	2024	$0.413
[58]	India	PV, WT, DG, and battery	2024	$0.403
[59]	Sri Lanka	PV and battery energy	2024	$0.366
[60]	Saudi Arabia	PV, battery, thermal, and hydrogen storage	2024	$0.252
[61]	West Africa	PV, battery, and biomass	2025	$0.202

DG = distributed generation; LCOE = levelized cost of energy; WT = wind turbine.

7.6. Comparative evaluation and discussion

To provide a more comprehensive assessment, a detailed comparison between the proposed battery-supercapacitor microgrid and the conventional grid-only system has been carried out across multiple performance dimensions:

- The system achieves a 50% renewable penetration level while ensuring uninterrupted supply under load demand uncertainty, as modeled using Gaussian-based load profiles. The energy management system effectively utilizes storage to maintain power balance with minimal reliance on the grid during peak demand periods.
- Although the calculated LCoE of the system, $0.11/kWh, is higher than the retail grid rate of $0.05/kWh, the total NPC is offset by substantial salvage value and operational cost savings through reduced fuel consumption and emissions. Table 7 presents a breakdown showing capital, maintenance, and replacement costs for each major component, highlighting the significant investment in wind and solar infrastructure compared to conventional grid use.
- The hybrid HESS strategy significantly reduces battery strain by pairing batteries with supercapacitors, which handle high-frequency charging-distribution cycles. This operational synergy increases the overall reliability of the system and prolongs the lifespan of the components, especially in volatile load profiles.
- The microgrid model supports decarbonization goals by leveraging 50% renewable energy, reducing emissions that would otherwise be generated under full reliance on fossil-fuel-based grid electricity.
- The use of probabilistic demand modeling and MEMS ensures the system adapts to real-time fluctuations, which is a capability typically absent in static conventional grids.

This comprehensive comparison not only underscores the feasibility of BSM under uncertain conditions but also provides stakeholders with a clear cost-benefit trade-off when transitioning toward sustainable energy systems.

7.7. Comparison with similar literature study

A comparative analysis of similar studies among some regional countries is provided in Table 8, as the different approach integration models are reported with their LCoE.

8. Conclusions

This research presented the optimal size and power exchange of a grid-connected microgrid incorporating solar panels, wind turbines, and a dual-layered HESS consisting of battery and super-capacitor technology, under real-world load demand uncertainty. A Gaussian distribution-based probabilistic model captures demand variability, while the system is managed by a logic-based algorithm and optimized using the GOA to minimize the overall operation cost and per unit cost of the energy. The proposed model achieves a 50% renewable energy penetration with an LCoE of *$0.11/kWh*, balancing cost-efficiency and carbon reduction. Results demonstrate that pairing batteries with

supercapacitors enhances responsiveness and longevity under intermittent conditions. The system reduces annual CO_2 emissions by approximately 88.41 kilotons compared to a fully grid-dependent baseline.

This integrated approach addresses the limitations of deterministic planning and single-layer storage, offering a scalable and resilient solution for clean energy deployment in developing nations. However, the irregular nature of renewable energy raises concerns about reliance on green resources. Another concern is that renewable generation is intermittent, meaning that energy output may vary from year to year. Future work may explore stochastic renewable generation profiles and adaptive control strategies to further enhance robustness.

CRediT authorship contribution statement

Md. Rashidul Islam: Conceptualization, Funding acquisition, Methodology, Supervision, Writing – original draft, Validation, Writing – review & editing. **Arafat Ibne Ikram:** Conceptualization, Formal analysis, Methodology, Resources, Software, Validation, Visualization, Writing – original draft, Writing – review & editing, Data curation. **Uddin Md. Ahad:** Conceptualization, Investigation, Methodology, Visualization, Writing – original draft, Writing – review & editing. **Rizvi Ahamed:** Formal analysis, Methodology, Visualization, Writing – original draft, Writing – review & editing.

Declaration of Competing Interest

The authors declared no conflict of interest.

References

[1] D. Akinyele, J. Belikov, Y. Levron, Challenges of microgrids in remote communities: a steep model application, Energies 11 (2) (2023) 432.

[2] A.S. Awad, T.H. El-Fouly, M.M. Salama, Optimal distributed generation allocation and load shedding for improving distribution system reliability, Electr. Power Compon. Syst. 42 (6) (2023) 576–584.

[3] S. Bouktif, A. Fiaz, A. Ouni, M.A. Serhani, Optimal deep learning lstm model for electric load forecasting using feature selection and genetic algorithm: comparison with machine learning approaches, Energies 11 (7) (2018) 1636.

[4] M. Saleem, S. Saha, U. Izhar, L. Ang, Optimized energy management of a solar battery microgrid: an economic approach towards voltage stability, J. Energy Storage 90 (2024) 111876.

[5] H. Yin, Y. Wang, G. Wu, Y. Liu, Y. Chen, J. Liu, Distributed optimal operation of pv-storage-load micro-grid considering renewable and load uncertainties, J. Energy Storage 86 (2024) 111168.

[6] X. Gong, X. Li, Z. Zhong, Strategic bidding of hydrogen-wind-photovoltaic energy system in integrated energy and flexible ramping markets with renewable energy uncertainty, Int. J. Hydrog. Energy 80 (2024) 1406–1423.

[7] I. Alam, A.I. Ikram, S.E.A. Himu, T. Khandaker, F. Abrar, N. Farzana, A cutting-edge implementation of iot-based monitoring for floating solar cells with dual-axis tracker, In: Proceedings of the 2023 IEEE 9th International Women in Engineering (WIE) Conference on Electrical and Computer Engineering (WIECON-ECE), IEEE, 2023. pp. 177-182.

[8] A.I. Ikram, M. Shafiullah, M.R. Islam, M.K. Rocky, Techno-economic assessment and environmental impact analysis of hybrid storage system integrated microgrid, Arab. J. Sci. Eng. 49 (12) (2024) 15917–15934, https://doi.org/10.1007/s13369-024-08735-x.

[9] J. Li, H. Wu, C. Zhu, M. Goh, Evaluating and analyzing renewable energy performance in oecd countries under uncertainty: a robust dea approach with common weights, Appl. Energy 375 (2024) 124115.

[10] Y. Lv, K. Li, H. Zhao, H. Lei, A multi-stage constraint-handling multi-objective optimization method for resilient microgrid energy management, Appl. Sci. 14 (8) (2024) 3253.

[11] A.S. Alghamdi, Microgrid energy management and scheduling utilizing energy storage and exchange incorporating improved gradient-based optimizer, J. Energy Storage 97 (2024) 112775.

[12] S. Rahim, Z. Wang, K. Sun, Adaptive robust framework for microgrid-integrated generation and network planning under uncertainty, Electr. Power Syst. Res. 237 (2024) 110955.

[13] G. Moorthy, S. Vijayalakshmi, A. Manjuladevi, M. Anusuya, Advanced energy management and power quality enhancement in hybrid fuel cell-battery-super capacitor microgrids using snow ablation optimizer-robust variational physics informed, J. Energy Storage 116 (2025) 115859.

[14] X. Zhang, Y. Yang, H. Zhao, Y. Luo, X. Xu, Two-stage optimal scheduling of an islanded microgrid considering uncertainties of renewable energy, Int. J. Electr. Power Energy Syst. 162 (2024) 110324.

[15] M.R. Khan, Z.M. Haider, F.H. Malik, F.M. Almasoudi, K.S.S. Alatawi, M.S. Bhutta, A comprehensive review of microgrid energy management strategies considering electric vehicles, energy storage systems, and ai techniques, Processes 12 (2) (2024) 270.

[16] A.I. Ikram, A. Ullah, D. Datta, A. Islam, T. Ahmed, Optimizing energy consumption in smart homes: Load scheduling approaches, IET Power Electron. 17 (2024) 2656–2668, https://doi.org/10.1049/pel2.12663.

[17] A.I. Ikram, M.S. Hassan, N. Akter, Electrical power quality disturbances detection in transmission lines using machine learning-enabled classifier, In: Proceedings of the 2024 International Conference on Advances in Computing, Communication, Electrical, and Smart Systems (iCACCESS), IEEE, 2024. pp. 1-6.

[18] M.S. Hassan, M.A. Siddique, N. Mohammad, A.I. Ikram, Performance analysis of machine learning-based traditional and ensemble techniques for smart grid stability prediction. In: Proceedings of the 2024 6th International Conference on Electrical Engineering and Information & Communication Technology (ICEEICT), IEEE, 2024. pp. 1020-1025.

[19] S.H. Kashfi, M.A. AlNoman, A.I. Ikram, S.E.A. Himu, F. Abrar, M. Rahman, M.I. UddinFeasibility study and performance analysis of rooftop solar panels and air-dolphin wind turbines. In: Proceedings of the 2023 5th International Conference on Sustainable Technologies for Industry 5.0 (STI), IEEE, 2023. pp. 1-6.

[20] A.I. Ikram, S.E.A. Himu, T. Khandaker, M.A.R. Reyad, A.W. Erfan, M.M. Alam, M.S. Islam, Design optimization and assessment of floating solar pv with wind turbine systems at kepz, In: Proceedings of the 2023 5th International Conference on Sustainable Technologies for Industry 5.0 (STI), IEEE, 2023. pp. 1-6.

[21] K.S. Sandhu, A. Mahesh, Optimal sizing of pv/wind/battery hybrid renewable energy system considering demand side management, Int. J. Electr. Eng. Inform. 10 (1) (2023) 79–93.

[22] S. Singh, S.C. Kaushik, Optimal sizing of grid integrated hybrid pv-biomass energy system using artificial bee colony algorithm, IET Renew. Power Gener. 10 (5) (2022) 642–650.

[23] P. Wang, W. Wang, D. Xu, Optimal sizing of distributed generations in dc microgrids with comprehensive consideration of system operation modes and operation targets, IEEE Access 6 (2023) 31129–31140.

[24] J. Abushnaf, A. Rassau, Impact of energy management system on the sizing of a grid-connected pv/battery system, Electr. J. 31 (2) (2023) 58–66.

[25] M.O. Badawy, F. Cingoz, Y. SozerBattery storage sizing for a grid tied pv system based on operating cost minimization. In: Proceedings of the 2016 IEEE Energy Conversion Congress and Exposition (ECCE), IEEE, 2022. pp. 1-7.

[26] O. Nadjemi, T. Nacer, A. Hamidat, H. Salhi, Optimal hybrid pv/wind energy system sizing: application of cuckoo search algorithm for algerian dairy farms, Renew. Sustain. Energy Rev. 70 (2022) 1352–1365.

[27] A.I. Ikram, S.E.A. Himu, R.A. Tahsin, M.M. Hoque, M.M. Alam, A.W. Erfan, N. Farzana, A grid-connected anfis-mppt based solar pv system and hybrid energy storage. In: Proceedings of the 2023 IEEE 9th International Women in Engineering (WIE) Conference on Electrical and Computer Engineering (WIECON-ECE), IEEE, 2023. pp. 30-35.

[28] M.S.-U. Islam, M.A.B. Zafar, M.R. Islam, A.I. Ikram, M. Shafiullah, Cost-effective optimal integration of renewable energy and waste-to-energy technologies, J. Eng. 2025 (1) (2025) e70148, https://doi.org/10.1049/tje2.70148.

[29] P. Kurukuri, M.R. Mohamed, P.H. Raavi, Y. Arya, Optimal planning and designing of microgrid systems with hybrid renewable energy technologies for sustainable environment in cities, Environ. Sci. Pollut. Res. 31 (22) (2024) 32264–32281.

[30] B.K. Reddy, N.C. Giri, P.K. Yemula, E.B. Agyekum, Y. Arya, Optimal operation of cogeneration power plant integrated with solar photovoltaics using dls-wma and ann, Int. J. Energy Res. 2024 (1) (2024) 5562804.

[31] A. Chadly, R.R. Urs, M. Wei, M. Maalouf, A. Mayyas, Techno-economic assessment of energy storage systems in green buildings while considering demand uncertainty, Energy Build. 291 (2023) 113130.

[32] A. Ashokkumar, N.A. Prabha, Energy management strategy for photovoltaic, fuel cell, battery, and super capacitor in standalone direct current microgrid system, J. Energy Storage 144 (2026) 119600.

[33] P. Jing, X. Zhang, A. Ukil, A. Swain, Faster joint control of battery and supercapacitor-based hess in dc microgrid using mpc with hybrid pi, J. Energy Storage 105 (2025) 114528.

[34] A.M. Abdurraqeeb, A.A. Al-Shamma'a, A. Alkuhayli, M. Alharbi, H.M.H. Farh, K.E. Addoweesh, Enhancing performance of supercapacitor based hybrid energy storage system using rst controller in an islanded dc microgrid, J. Energy Storage 113 (2025) 115522.

[35] M.R. Babaei, A. Ghasemi-Marzbali, S. Abbasalizadeh, Control of a combined battery/supercapacitor storage system for dc microgrid application, J. Energy Storage 96 (2024) 112675.

[36] E. Hassaballah, H. Keshta, K. Abdel-Latif, A. Ali, A novel strategy for real-time optimal scheduling of grid-tied microgrid considering load management and uncertainties, Energy 299 (2024) 131419.

[37] S. Zhou, Y. Han, A.S. Zalhaf, M. Lehtonen, M.M. Darwish, K. Mahmoud, A novel stochastic multistage dispatching model of hybrid battery-electric vehicle-supercapacitor storage system to minimize three-phase unbalance, Energy 296 (2024) 131174.

[38] M. Žnidarec, D. Šljivac, G. Knežević, H. Pandžić, Double-layer microgrid energy management system for strategic short-term operation scheduling, Int. J. Electr. Power Energy Syst. 157 (2024) 109816.

[39] N.A. Siddiqui, H. Tahir, M. Akram, H.U. Manzoor, Optimized control of hybrid energy storage systems using whale optimization algorithm for enhanced battery longevity and stability in microgrids, Eng. Rep. 7 (5) (2025) e70199.

[40] A. Fathy, S.A. Alfayyadh, Efficient energy management strategy for reducing the hydrogen consumption of hybrid fuel cell/supercapacitor/battery microgrid, Int. J. Hydrog. Energy 162 (2025) 150715.

[41] A. Criollo, D. Benavides, P. Arévalo, L.I. Minchala-Avila, D. Morales-Jadan, Enhancing grid stability in microgrid systems with vehicle-to-grid support and edlc supercapacitors, Batteries 11 (6) (2025) 231.

[42] M. Gharibi, A. Askarzadeh, Size and power exchange optimization of a grid-connected diesel generator-photovoltaic-fuel cell hybrid energy system considering reliability, cost and renewability, Int. J. Hydrog. Energy 44 (47) (2023) 25428–25441.
[43] A. Tabak, E. Kayabasi, M.T. Guneser, M. Ozkaymak, Grey wolf optimization for optimum sizing and controlling of a pv/wt/bm hybrid energy system considering tnpc, lpsp, and lcoe concepts, Energy Sources Part A Recovery Util. Environ. Eff. 44 (1) (2022) 1508–1528.
[44] A.M. Abdelshafy, H. Hassan, J. Jurasz, Optimal design of a grid-connected desalination plant powered by renewable energy resources using a hybrid pso–gwo approach, Energy Convers. Manag. 173 (2023) 331–347.
[45] Power Cell Govt. of BD, 2025. ⟨http://www.powercell.gov.bd/⟩. (Accessed January 24, 2025).
[46] B. Dey, L.K. Chanu, G. Sharma, P.N. Bokoro, A comprehensive techno-economic analysis for a phev-integrated microgrid system involving wind uncertainty and diverse demand side management policies, Results Eng. 26 (2025) 105176.
[47] Z. Qiu, Z. Zhu, L. Yu, Z. Han, W. Shao, K. Zhang, Y. Ma, Robust optimal operation of smart microgrid considering source–load uncertainty, Processes 13 (8) (2025) 2458.
[48] W. Liu, W. Yan, T. Li, G. Han, T. Ren, A multi-strategy improved grasshopper optimization algorithm for solving global optimization and engineering problems, Int. J. Comput. Intell. Syst. 17 (1) (2024) 182.
[49] M. Jabari, A. Rad, M.A. Nasab, M. Zand, S. Padmanaban, S. Muyeen, J.M. Guerrero, Parameter identification of pv solar cells and modules using bio dynamics grasshopper optimization algorithm, IET Gener. Transm. Distrib. 18 (21) (2024) 3314–3338.
[50] X. Yu, P. Zunu, An enhanced grasshopper optimization algorithm with outpost and multi-population mechanisms for dolomite lithology prediction, Biomimetics 10 (8) (2025) 494.
[51] K. Kalita, P. Jangir, R. Čep, S.B. Pandya, L. Abualigah, Many-objective grasshopper optimization algorithm (maogoa): a new many-objective optimization technique for solving engineering design problems, Int. J. Comput. Intell. Syst. 17 (1) (2024) 214.
[52] A.I. Abeg, M.R. Islam, M.A. Hossain, M.F. Ishraque, M.R. Islam, M. Hossain, Capacity and operation optimization of hybrid microgrid for economic zone using a novel meta-heuristic algorithm, J. Energy Storage 94 (2024) 112314.
[53] B. Khan, P. Singh, Selecting a meta-heuristic technique for smart micro-grid optimization problem: a comprehensive analysis, IEEE Access 5 (2017) 13951–13977.
[54] S. Saremi, S. Mirjalili, A. Lewis, Grasshopper optimisation algorithm: theory and application, Adv. Eng. Softw. 105 (2022) 30–47.
[55] NASA, Nasa's prediction of worldwide energy resources (power), 2023. ⟨https://www.pgcb.gov.bd/⟩.
[56] A.K. Karmaker, M.M. Rahman, M.A. Hossain, M.R. Ahmed, Exploration and corrective measures of greenhouse gas emission from fossil fuel power stations for bangladesh, J. Clean. Prod. 244 (2020) 118645.
[57] H.M. El Zoghby, A.F. Bendary, R.S. Afia, et al., Techno-economic study of a 100% renewable energy-based isolated microgrid involving green hydrogen production, Sustain. Energy Technol. Assess. 76 (2025) 104303.
[58] A. Naseem, I. Ashraf, M.M. Kamal, Designing and optimisation of microgrid with green energy source for efficient power supply. In: Proceedings of the International Conference on ICT for Digital, Smart, and Sustainable Development, Springer, 2024. pp. 57-71.
[59] S. Forrousso, S.I. Kaitouni, A. Mana, M. Wakil, A. Jamil, J. Brigui, H. Azzouzi, Optimal sizing of off-grid microgrid building-integrated-photovoltaic system with battery for a net zero energy residential building in different climates of morocco, Results Eng. 22 (2024) 102288.
[60] A. Alemam, A.S. Al-Sumaiti, I. Afgan, Optimized hybrid storage standalone microgrid with electrical, heat, and hydrogen loads based on stochastic photovoltaic modelling, Energy Convers. Manag. X 27 (2025) 101091.
[61] I. Amoussou, M.R. Aza-Gnandji, M. Kplé, A. Didavi, T.C. Nounangnonhou, C.W. Adihou, M. Agbomahéna, F.-X. Fifatin, Optimizing an autonomous microgrid based on renewable energy systems for rural electrification in benin, Available at SSRN 5101048, 2025.